THE JOURNAL OF PHYSICAL CHEMISTRY A
A JOURNAL OF THE AMERICAN CHEMICAL SOCIETY

pubs.acs.org/JPCA

Article

Transition Temperature for Spin-Crossover Materials with the Mean Value Ensemble Hubbard-*U* Correction

Angel Albavera-Mata, Richard G. Hennig,* and S. B. Trickey*

Cite This: *J. Phys. Chem. A* 2023, 127, 7646−7654

Read Online

ACCESS | Metrics & More | Article Recommendations

ABSTRACT: Calculation of transition temperatures $T_{1/2}$ for thermally driven spin-crossover in condensed phases is challenging, even with sophisticated state-of-the-art density functional approximations. The first issue is the accuracy of the adiabatic crossover energy difference ΔE_{HL} between the low- and high-spin states of the bistable metal−organic complexes. The other is the proper inclusion of entropic contributions to the Gibbs free energy from the electronic and vibrational degrees of freedom. We discuss the effects of treatments of both contributions upon the calculation of thermochemical properties for a set of 20 spin-crossover materials using a Hubbard-*U* correction obtained from a reference ensemble spin-state. The *U* values obtained from a simplest bimolecular representation may overcorrect, somewhat, the ΔE_{HL} values, hence giving somewhat excessive reduction of the $T_{1/2}$ results with respect to their $U = 0$ values in the crystalline phase. We discuss the origins of the discrepancies by analyzing different sources of uncertainties. By use of a first-coordination-sphere approximation and the assumption that vibrational contributions from the outermost atoms in a metal−organic complex are similar in both low- and high-spin states, we achieve $T_{1/2}$ results with the low-cost, widely used PBE generalized gradient density functional approximation comparable to those from the more costly, more sophisticated r^{2}SCAN meta-generalized gradient approximation. The procedure is promising for use in high-throughput materials screening, because it combines rather low computational effort requirements with freedom from user manipulation of parameters.

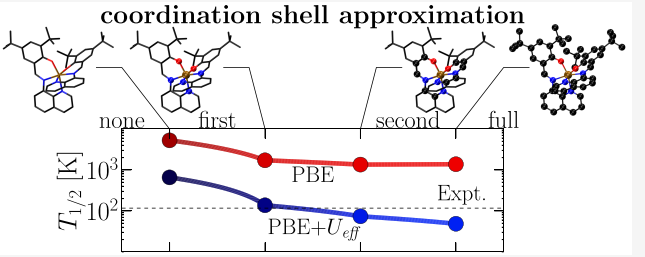

INTRODUCTION

Spin-crossover transitions may be seen as the result of additive collective inter- and intramolecular effects arising from an ensemble of molecular units in a sample.[1] Crossovers usually are classified as gradual, abrupt, and stepped. They can be either complete or incomplete.[2] For the thermodynamic limit of weakly coupled molecules, the total magnetic moment is the ensemble average over the local magnetic moments from all molecules in the system.[3] Starting at low temperatures, a typical crossover material has a vast majority of the molecules in such an ensemble in the low-spin (LS) state. As the temperature rises, the individuals switch to a high-spin (HS) state until an equilibrium is reached, with an equal population of molecules in LS and HS states in an ideal solution model. At that point, the Gibbs free energy difference for the two populations is zero. Further increase in temperature continues the conversion until the vast majority of the population reaches the HS state. The analogous picture holds for the reverse situation, with the two paths sometimes differentiated by hysteresis resulting from differing conversion energetics.[4,5] For the spin conversion phenomenon, one can define the transition temperature at population equilibrium as $T_{1/2} = \Delta H/\Delta S$, calculated from the enthalpy and entropy differences, ΔH and ΔS, respectively, along the heating or cooling paths.[6−9]

A contemporary experimental goal is to find appropriate combinations of transition metals and ligands to give a $T_{1/2}$ value at or close to room temperature.[10−20] Pursuit of operation at or near ambient temperature, rather than low temperatures, is motivated by the prospect of myriad applications of these materials as actuators, displays, sensors, memory storage, magnetic resonance imaging, spintronics, or molecular electronics.[21−34] Understanding the effects of the physical and chemical characteristics of the ligand choice upon the spin transition is key to guiding the design of materials with such tailored properties.[35]

For that endeavor, the Kohn−Sham density functional electronic structure scheme[36] offers an efficient, yet competitive, alternative to wave function or perturbation-based methods for property computation. The accuracy of the Kohn−Sham total energy is influenced, strongly, by the choice of exchange-correlation density functional approximation. In

Received: May 24, 2023
Revised: August 22, 2023
Published: September 5, 2023

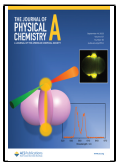

https://doi.org/10.1021/acs.jpca.3c03520
J. Phys. Chem. A 2023, 127, 7646−7654

large-scale materials calculations, computational cost-effectiveness is a strong motivation for use of generalized or meta-generalized gradient density functional approximations.[37] Those have shortcomings for the treatment of d-electrons. They, of course, have a central role in spin equilibrium molecules. In quantum chemistry those shortcomings often are addressed by mixing such functionals with a fraction of single-determinant exchange to yield global,[38] range-separated,[39,40] and local hybrids.[41] Because of computational cumbersomeness, condensed matter applications often resort to the Hubbard model[42] for the needed corrections via the so-called DFT+U approach.[43]

Meaningful use of comparatively cost-effective approximations obviously should deliver $T_{1/2}$ values comparable to the experimental ones, preferably without requiring intervention or manipulation. As noted, the thermodynamic potential relevant to thermally driven spin conversion is the LS-to-HS Gibbs free energy change. Assuming that the intermolecular coupling in the material depends only weakly on the molecular spin-states, the Gibbs free energy of the material is expressed by an ideal solution model that includes the Gibbs free energy of the individual molecules in the LS and HS states and the ideal entropy of mixing, to wit

$$G = \alpha_{HS} G_{HS} + (1 - \alpha_{HS}) G_{LS} - TS_{mix} \quad (1)$$

Here α_{HS} denotes the fraction of HS states and the entropy of mixing is

$$S_{mix} = -k_B N_A (\alpha_{HS} \ln[\alpha_{HS}] + (1 - \alpha_{HS}) \ln[1 - \alpha_{HS}]) \quad (2)$$

N_A is Avogadro's number and k_B is the Boltzmann constant. The thermal evolution of the spin transition in eq 1 can be described via the equilibrium condition[44]

$$\left(\frac{\partial G}{\partial \alpha_{HS}}\right)_{T,P} = 0 \quad (3)$$

$$= \Delta E_{HL} + \Delta F_{vib} + P\Delta V - T\Delta S_{ele} - k_B N_A T \ln\left[\frac{1 - \alpha_{HS}}{\alpha_{HS}}\right] \quad (4)$$

with $\alpha_{HS} = 1/2$ at $T_{1/2}$, determined through a numerical method. The key energy difference, $\Delta E_{HL} = E_{HS} - E_{LS}$, is the adiabatic molecular crossover energy calculated from the total energy difference between the high- and low-spin configurations, E_{HS} and E_{LS}, respectively. The vibrational free energy difference between the LS and HS states, $\Delta F_{vib} = \Delta E_{vib} - T\Delta S_{vib}$, includes the terms ΔE_{vib} and ΔS_{vib} from the vibrational contributions to the energy and entropy, respectively, that depend nonlinearly on T. Those are readily obtainable from a set of independent harmonic oscillators on the normal coordinates of the molecule. See ref 45 for detailed expressions. Since the enthalpy contribution from the volume expansion is smaller at atmospheric pressure, we neglect the term $P\Delta V$. In addition, $\Delta S_{ele} = \Delta S_{spin} + \Delta S_{orb} + \Delta S_{Fermi}$, where the leading term is the spin entropy $\Delta S_{spin} = k_B N_A \ln[(2S_{HS} + 1)/(2S_{LS} + 1)]$ associated with the change in total spin S_{LS}-to-S_{HS}, whereas the entropy variation due to orbital degeneracy, ΔS_{orb}, and Fermi entropy, ΔS_{Fermi}, usually are neglected.

As already noted, the narrow d-bands that are central to the properties of bistable materials usually are not described well by comparatively simple density functional approximations. That shortcoming has motivated extensive investigation of hybrid density functionals for the calculation of spin crossover in isolated molecules.[46−55] As a matter of context, we remark that proper Kohn−Sham evaluation of hybrid approximations requires use of the optimized effective potential.[56−58] That, however, is not the customary choice because of the significant computational resources required. Instead, the generalized Kohn−Sham procedure almost always is used with such exchange-correlation approximations. Even that choice, however, has significance for the purpose of computational screening of crystalline phases of crossover materials because the evaluation of single-determinant exchange with a plane-wave basis set is computationally costly and because methods such as projector augmented waves for reducing the cost have not been developed for hybrid functionals.

Those drawbacks are circumvented reasonably effectively by correcting relatively simple exchange-correlation approximations with Hubbard-U treatment of the d-electrons. Application of the scheme to thermodynamics and the calculation of $T_{1/2}$ have been reported.[59−63] Because the cornerstone of this approximation is the magnitude of the U and J parameters for the interactions between parallel and anti-parallel spins, there is active research on devising methodologies for determining appropriate, or better suited, U and J without steering or fitting to experimental data.[64−68]

In the setting of spin crossover, unfortunately those methods can give drastically inaccurate U values or fail to give any meaningful value at all.[69] To address that, recently we introduced an effective Hubbard-U correction, $U_{eff} = U - J$, determined from a spin-state built from a linearly mixed ensemble of the pure LS and HS states.[70] Compared with the uncorrected density functional approximation, the methodology improves, significantly, the calculated ΔE_{HL} values for a representative set of metal−organic molecules. The present work extends our analysis to the calculation of $T_{1/2}$ of crystalline phases of spin transition materials via the use of the U_{eff} values from that new methodology. We start by comparing the differences in the calculated ΔE_{HL} for solids versus molecules and later focus our attention solely on the materials. We discuss the influence of uncertainties on our choice of methodology and the possibility of computing $T_{1/2}$ by restricting vibrational entropic contributions to those from the harmonic frequencies from the metallic core of the metal−organic complex. That approximation assumes that the rest of the vibrational contributions largely cancel between the spin-states. For the widely used, simple PBE exchange-correlation approximation,[71,72] results for PBE+U_{eff} with this methodology suggest an encouraging compromise between accuracy and speed, a combination we deem to be attractive for high-throughput strategies that make use of intensive computing resources. Note that our goal is not exact reproduction of the experimental transition temperature but rather the ability to screen thousands of candidates with low computing effort and in reasonable timings using simple estimates of $T_{1/2}$. Finally, we notice that utilization of U_{eff} values derived from the simplest molecular representation of the ensemble may overcorrect the calculated ΔE_{HL} for solids. That, as we show by an example, leads to an underestimation of $T_{1/2}$ when all of the degrees of freedom for a representative test case are considered. Arguably because those U_{eff} values are calculated only on molecules, they take account only of intramolecular interactions and lack information about the intermolecular interactions characteristic of the crystalline phase.

https://doi.org/10.1021/acs.jpca.3c03520
J. Phys. Chem. A 2023, 127, 7646−7654

COMPUTATIONAL DETAILS

The test set of complexes we considered and their reported $T_{1/2}$ values are given in Table 1. The set consists of 20 species[52,73] distributed as one Cr^{II}, three each of Mn^{III}, Mn^{II}, and Fe^{III}, and five each of Fe^{II} and Co^{II} ions. It is a subset of the test set used in ref 70, comprised of those complexes with a reported $T_{1/2}$.

Table 1. Metal−Organic Complexes in the Test Set Sorted by Metallic Ion[a]

Complex	Ion	Ref.	U_{eff}	$T_{1/2}$
$[Cr(I_2)(depe)_2]$	Cr^{II}	74	31.13 (1.35)	171
$[Mn(L_1tren)]$	Mn^{III}	75	29.52 (1.28)	40−50
$[Mn(3,5\text{-diBr-sal}_2323)][BF_4]$	Mn^{III}	76	29.06 (1.26)	175
$[Mn(L_2)][PF_6]$	Mn^{III}	77	29.29 (1.27)	131
$[Mn(Cp^{1\text{-Me}})_2]$	Mn^{II}	78	25.83 (1.12)	303
$[Mn(Cp^{1\text{-}t\text{Bu}})_2]$	Mn^{II}	79	26.06 (1.13)	215
$[Mn(Cp^{1,3\text{-}t\text{Bu}})_2]$	Mn^{II}	79	26.29 (1.14)	300
$[Fe(acac)_2(trien)][PF_6]$	Fe^{III}	80	44.51 (1.93)	200
$[Fe(qsal\text{-}Br)_2][NO_3]$	Fe^{III}	81	46.35 (2.01)	232
$[Fe(3\text{-OMe-salen})_2][PF_6]$	Fe^{III}	82	44.97 (1.95)	164
$[Fe(phen)_2(NCS)_2]$	Fe^{II}	83	46.81 (2.03)	177
$[Fe(stpy)_2(NCS)_2]$	Fe^{II}	84	47.50 (2.06)	109
$[Fe(bpp)_3][BF_4]_2$	Fe^{II}	85	44.28 (1.92)	256
$[Fe(H_2B(pz)_2)_2(bipy)]$	Fe^{II}	86	46.58 (2.02)	160
$[Fe(tzpy)_2(NCS)_2]$	Fe^{II}	87	47.04 (2.04)	118
$[Co(terpyridine)_2]$	Co^{II}	88	38.28 (1.66)	200
$[Co(H_2(fsa)_2en)(Py)_2]$	Co^{II}	89	36.67 (1.59)	121
$[Co(terpyrindone)_2][ClO_4]_2$	Co^{II}	90	37.36 (1.62)	172
$[Co(papl)_2]$	Co^{II}	91	38.28 (1.66)	150
$[Co(MeO\text{-terpy})_2][BF_4]_2$	Co^{II}	92	36.90 (1.60)	250

[a]The experimental transition temperatures, taken from refs 52 and 73, are in Kelvin. The effective Hubbard-U, $U_{eff} = U - J$, are in kcal/mol (eV) and are from ref 70. depe = 1,2-bis(diethylphosphino)ethane, L_1tren = tris(2-((pyrrol-2yl)methyleneamino)ethyl)amine, 3,5-diBr-sal$_2$323 = 2,2′-(2,6,9,13-tetraazatetradeca-1,13-diene-1,14-diyl)bis-(4,6-dibromophenolato), L_2 = (2,2′-(2,6,9,13-tetraazatetradeca-1,13-diene-1,14-diyl)diphenol), $Cp^{1\text{-Me}}$ = methylcyclopentadiene, $Cp^{1\text{-}t\text{Bu}}$ = *tert*-butylcyclopentadienyl, $Cp^{1,3\text{-}t\text{Bu}}$ = *tert*-butylcyclopenta-1,3-diene, acac = acetylacetonate, trien = triethylenetetramine, qsal-Br = (N-8-quino-lyl)-5-Br-salicylaldiminate, 3-OMe-salen = (2-(((2-(ethylamino)ethyl)imino)methyl)-6-methoxyphenolato-N,N′,O), phen = phenanthroline, stpy = 4-styrylpyridine, bpp = (2,6-di(pyrazol-1-yl)pyridine), $H_2B(pz)_2$ = dihydrogen bis(pyrazol-1-yl)borate, bipy = bipyridine, tzpy = (3-(2-pyridyl)(1,2,3)triazolo(1,5-a)pyridine), $H_2(fsa)_2$en = 3-formylsalicylic acid-ethylendiamine, papl = 1-(2-pyridylazo)-2-phenanthrol, MeO-terpy = 4′-methoxy-2,2′:6′-terpyridine.

All calculations were done with VASP 6.2[93] with the generalized gradient approximation PBE and meta-generalized gradient approximation r^{2}SCAN exchange-correlation density functionals.[71,72,94] For PBE+U_{eff}, we used the effective Hubbard-U values from ref 70 shown in Table 1. These were obtained following the steps depicted in Figure 1 using the mean value ensemble methodology from a bimolecular sample of the solid. The choice of projector augmented wave potentials was the same as that in ref 70. The plane-wave kinetic energy cutoff was set to 600 eV, with an auxiliary support grid used for evaluation of the augmentation charges. Nonspherical corrections to the electron density gradient were included, and the precision tolerance was set to the choice labeled accurate. The threshold for self-consistent field convergence was set to 10^{-6} eV and tightened to 10^{-7} eV for the calculation of harmonic frequencies. Those were calculated through a finite differences approach with a step size of 10^{-2} Å. The Gaussian smearing width was chosen as 10^{-3} eV. The geometries of the crystalline phases were optimized with the conjugate gradient algorithm until forces were smaller than 10^{-3} eV Å^{-1}, using a k-point density of 0.2 Å^{-1}, and the Γ q-point for phonon computations. Single molecules were calculated with the same set of computational choices. We placed them in orthorhombic boxes with at least 10 Å of vacuum in each direction but used the Γ point to calculate the total energy.

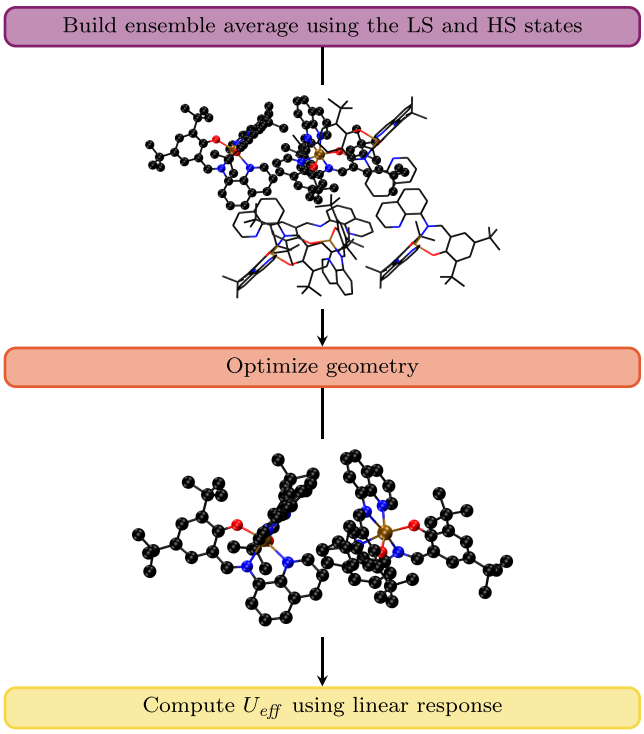

Figure 1. Workflow used in ref 70 for the calculation of the Hubbard-U_{eff} value for each of the spin-crossover complexes. From the top, first is isolation of the bimolecular sample from a supercell, second is geometry relaxation for that sample, and third is determination of U_{eff} using a linear response procedure.[65]

Transition temperatures were treated by considering the thermal evolution of the Gibbs free energy difference as a function of temperature and solving eq 4 numerically to determine $T_{1/2}$.

RESULTS AND DISCUSSION

We begin by focusing our discussion on the key contribution to eq 4 for a proper description of the spin transition, namely, the adiabatic total energy difference ΔE_{HL}. Figure 2a illustrates the behavior of ΔE_{HL} when calculated on the molecular complex or the crystalline phase. The first thing to note is that the choice of density functional matters, as does the choice of sample representation, isolated molecule versus crystalline. A meta-GGA such as r^{2}SCAN delivers a balanced description of molecules and their condensed phases. This balanced behavior is well documented in the literature.[94] In contrast, a GGA such as PBE provides better results for molecules than for solids in the form of smaller, thus more realistic, ΔE_{HL}. The counterpart parametrization for solids, PBEsol,[95,96] behaves oppositely to PBE. Perhaps unsurprisingly, PBEsol+U is competitive with

https://doi.org/10.1021/acs.jpca.3c03520
J. Phys. Chem. A 2023, 127, 7646−7654

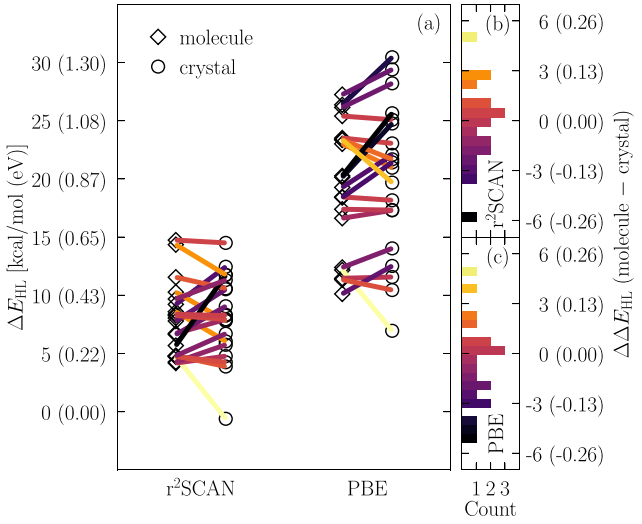

Figure 2. (a) Adiabatic spin-crossover energies, $\Delta E_{HL} = E_{HS} - E_{LS}$, calculated on the molecular complexes and their respective crystalline phases, with both the PBE and r^{2}SCAN density functionals. (b, c) Distribution of the deviation $\Delta\Delta E_{HL}$ for ΔE_{HL} calculated on a molecular representation and the solid for both density functionals. The color gradient in all panels depicts the magnitude of the difference between the results obtained on the molecule and the crystalline phase.

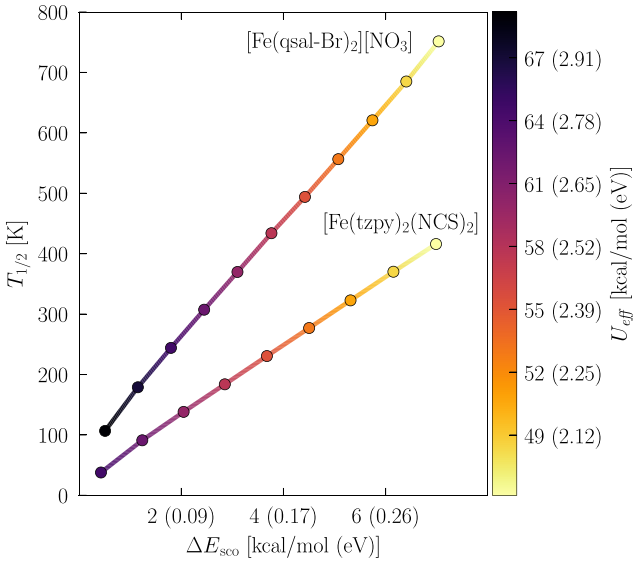

Figure 3. Correlation between the transition temperature $T_{1/2}$, in Kelvin, and the spin-crossover energy $\Delta E_{sco} = \Delta E_{HL} + \Delta E_{zpe}$, in units of kcal/mol (eV), corrected with the zero-point energy ΔE_{zpe}, for the crystalline phases of the [Fe(qsal-Br)$_2$][NO$_3$] and [Fe(tzpy)$_2$(NCS)$_2$] spin transition materials, for 46.12 kcal/mol $\leq U_{eff} \leq$ 69.18 kcal/mol (2 eV $\leq U_{eff} \leq$ 3 eV).

PBE+U when appropriate empirical U values are used.[97,98] The overwhelming popularity of PBE however compels the use of it in this case.

Second, parts b and c of Figure 2 also show that ΔE_{HL} computed on molecules and condensed phases differs by as much as about ±5.77 kcal/mol (±250 meV), with the largest discrepancies corresponding to [Cr(I$_2$)(depe)$_2$] and [Fe(tzpy)$_2$(NCS)$_2$] for both density functionals. In general, the mean absolute deviation on the 20-complex $T_{1/2}$ data set is 2.2 and 1.87 kcal/mol (95 and 81 meV) for PBE and r^{2}SCAN, respectively. By considering these mean deviations, a $\Delta\Delta E_{sco}$ value of ∼2.3 kcal/mol (100 meV) accounts for an uncertainty in $\Delta T_{1/2}$ of ∼100−150 K, as extracted from the correlation between these two quantities for different choices of U_{eff} in Figure 3, taking [Fe(qsal-Br)$_2$][NO$_3$] and [Fe(tzpy)$_2$(NCS)$_2$] as illustrative examples. Several reasons may account for the differences between results on molecules and solids. For instance, isolated molecules have fewer steric constraints compared to the condensed phase; hence, the number of accessible conformers for an isolated molecule is larger than those for a molecule in the aggregate. Conversely, an isolated molecule obviously accounts only for intramolecular interactions and evidently does not represent the cooperative interactions intrinsic to solid binding.

Intermolecular collectivity, however, is important in thermally driven spin-state transitions. Indeed, most of what is known experimentally about spin conversion is from the investigation of solid phases. Therefore, we studied the contributions to ΔF_{vib} in eq 4, as related to the harmonic vibrational frequencies, and their behavior with respect to different choices of coordination sphere approximations. A particular objective was to find a good compromise between the computing effort and accuracy. We classified vibrational contributions into four groups:

- Δ_ν^0 - The zeroth approximation, with $\Delta F_{vib} = 0$. The vibrational contributions are neglected.
- Δ_ν' - The first coordination sphere approximation, with $\Delta F'_{vib}$ calculated from the harmonic frequencies using the transition metal center and the first atoms coordinated to it, while keeping the rest of the atoms in the unit cell at fixed positions.
- Δ_ν'' - The second coordination sphere approximation, with $\Delta F''_{vib}$ calculated from the harmonic frequencies using the transition metal center and up to the second atoms coordinated to it or, if possible, the first closed rings surrounding the metal center, whereas the rest of the atoms in the unit cell remain fixed in place.
- Δ_ν - The full set of vibrational frequencies, as in eq 4, that accounts for all the degrees of freedom from the atoms in the unit cell.

To gain insight into the relative importance of these contributions without relying upon complexes in the test set, which implicitly would be equivalent to calibrating to them, we considered an additional system, not in the test set, namely, the homoleptic complex [Fe(*t*Bu$_2$qsal)$_2$] with the asymmetric tridentate ligand *t*Bu$_2$qsal = 2,4-di(*tert*-butyl)-6-((quinoline-8-ylimino)methyl)phenol.[99]

Figure 4 compares the four Δ_ν approximations for [Fe(*t*Bu$_2$qsal)$_2$] computed with PBE and PBE+U_{eff} with U_{eff} = 47 kcal/mol (2.04 eV) from ref 70. The convergence for $\Delta E_{sco} = \Delta E_{HL} + \Delta E_{zpe}$, including the zero-point energy ΔE_{zpe}, in going from Δ_ν^0 to Δ_ν is depicted in Figure 4a. Note that these contributions to the Gibbs free energy do not depend on T. Results show that the first coordination sphere approximation Δ_ν' captures most of the vibrational contributions to ΔE_{zpe} for this complex, with ΔE_{sco} differing by 0.52 and 0.59 kcal/mol (22 and 26 meV) for PBE and PBE+U_{eff}, respectively, with respect to the result Δ_ν using the full degrees of freedom in the material. Overall, since ΔE_{sco} is smaller than 2.3 kcal/mol (100 meV) for the PBE+U_{eff} treatment, the associated

https://doi.org/10.1021/acs.jpca.3c03520
J. Phys. Chem. A 2023, 127, 7646−7654

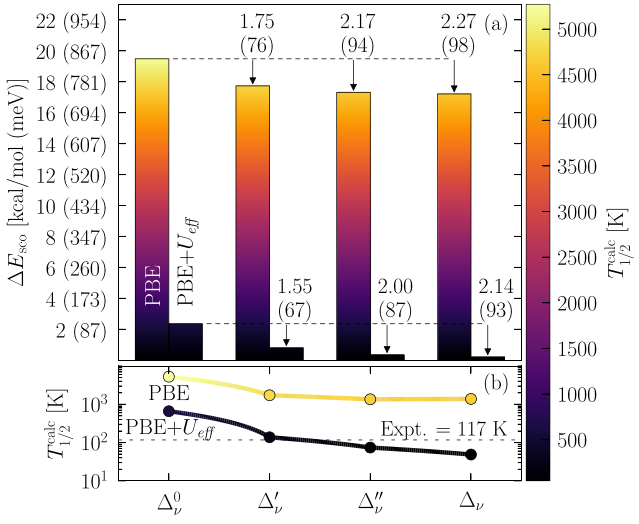

Figure 4. Dependence of (a) $\Delta E_{sco} = \Delta E_{HL} + \Delta E_{zpe}$ and (b) $T_{1/2}$, obtained from eq 4, upon the number of coordination shells included in the determination of the vibrational contributions for both PBE and PBE+U_{eff} for the crystalline phase of the complex $[Fe(tBu_2qsal)_2]$. U_{eff} = 47 kcal/mol (2.04 eV) is from ref 70. Panel (a) displays ΔE_{sco} values in kcal/mol (meV) vertically in the bars for PBE or above them for PBE+U_{eff}. The arrows depict the decrease in ΔE_{sco} due to ΔE_{zpe} for a given coordination shell approximation relative to the Δ_ν^0 values. In both panels, the color gradient illustrates the associated $T_{1/2}$.

uncertainty on the calculated $T_{1/2}$ is expected to be important for the use of that approximation. Hence, turning to the calculated $T_{1/2}$, Figure 4b depicts behavior parallel to that of ΔE_{sco} with both density functional approximations, but here we further consider the magnetic and vibrational contributions to G that depend on T. The $T_{1/2}$ with any of the four Δ_ν-type approximations in conjunction with PBE is overestimated by essentially an order of magnitude with respect to the experimental reference of 117 K. In contrast, PBE+U_{eff} goes from overestimating to underestimating $T_{1/2}$ in going from Δ_ν^0 to Δ_ν. What this shows is that the mean-value ensemble utilized with the simplest molecule-only ensemble gives a U_{eff} that is oversized when used in the condensed phase vibrational context. The underestimation of $T_{1/2}$ is due to the oversized U_{eff} for $[Fe(tBu_2qsal)_2]$. That, in turn, can be compensated by using the Δ_ν' approximation, with $T_{1/2}$ results in close agreement with experiment.

That compensation again raises the issue of uncertainties. The U_{eff} values reported in ref 70 were obtained only from the two closest molecules in a supercell. One expects, therefore, those values to be biased toward molecular properties in the sense that they neglect, entirely, crystal field effects upon spin crossover. That neglect leads to oversized U_{eff} values for solids. More specifically, the methodology discussed in ref 70 results in uncertainties of approximately ±2.3 kcal/mol (±100 meV) for the calculated U_{eff} that, in turn, manifest themselves roughly as an accumulated 50 K uncertainty on $T_{1/2}$. For PBE+U_{eff} in particular, the message in Figure 4 is clear. Oversized U_{eff} values may be obtained from a mean value ensemble spin reference. The overly large magnitude, though seemingly useful for ΔE_{HL} comparisons, can overcorrect the calculated $T_{1/2}$ value for $[Fe(tBu_2qsal)_2]$ when considering all degrees of freedom as in the Δ_ν case. We argue that one of the main causes of this behavior involves the choice of representation used to determine U_{eff} and the associated uncertainty on the calculation of $T_{1/2}$. A way to counteract part of the overcorrection for solids would be to build a reference spin-state for the mean-value ensemble that uses a supercell formed by the cluster expansion approximation.[100−103] That, however, would implicate substantial, possibly prohibitive, additional computational cost as well as the need to determine a reliable protocol independent of user intervention. Those issues go far beyond the scope of this work.

That same reasoning makes it plausible, at least, that there is a range of coordination shells such that the change in $T_{1/2}$, due to the uncertainty in U_{eff}, is similar to the difference in ΔF_{vib} for distinct choices of shells. The uncertainty magnitude is, however, system specific. That motivates the use of the first coordination sphere approximation, Δ_ν'. It avoids the need for more expensive approximations to ΔF_{vib}, due to the intrinsic uncertainty in ΔE_{sco} from the choice of density functional and the U_{eff} associated with the methodology. Our ansatz further assumes that contributions to G from the frequency-dependent terms can be neglected as one moves away from the metallic core, a result of near cancellation between the LS and HS states. Therefore, it is highly plausible that the leading terms contributing to $T_{1/2}$ are dominated primarily by the differences of the vibrational frequencies from the atoms directly coordinated to the transition metal, as is the case in the Δ_ν' approximation.

On the basis of the foregoing rationale, we used the Δ_ν' approximation to calculate $T_{1/2}$ for the metal−organic complexes in the test set. Figure 5 shows that the transition

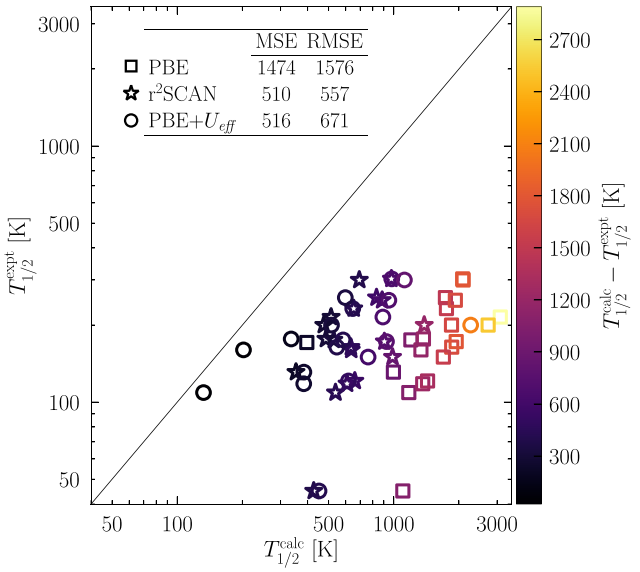

Figure 5. Correlation between calculated transition temperatures, $T_{1/2}^{calc}$, with the PBE, r^{2}SCAN, and PBE+U_{eff} density functional approximations and the reported experimental values, $T_{1/2}^{expt}$, using a continuous black line to depict the full correlation between both quantities. A first coordination sphere for the harmonic vibrational modes was employed for $\Delta F_{vib}'$. The mean signed error, MSE, and root-mean-square error, RMSE, are reported in units of Kelvin.

temperatures calculated on the crystalline phases using the PBE density functional are on the order of 10^3 K, whereas the experimental references are on the order of 10^2 K. The set of $T_{1/2}$ values calculated with the more sophisticated r^{2}SCAN improves over PBE. We alert the reader that $T_{1/2}$ results for the

https://doi.org/10.1021/acs.jpca.3c03520
J. Phys. Chem. A 2023, 127, 7646−7654

crystalline phase of $[Cr(I_2)(depe)_2]$ are not reported for r^{2}SCAN nor PBE+U_{eff} because they predict a negative ΔE_{sco}.

Different behaviors are observed for PBE+U_{eff}. Figure 5 shows that this approximation reduces the overestimation in $T_{1/2}$ with respect to the values obtained with PBE and competes in accuracy with the more sophisticated r^{2}SCAN density functional, with mean signed errors of 516 and 510 K, and root-mean-square errors of 671 and 557 K, for PBE+U_{eff} and r^{2}SCAN, respectively. See the inset in Figure 5. The PBE +U_{eff} approximation, therefore, is a quantitative improvement over the uncorrected PBE density functional. Though the results still are not quantitatively accurate on a system by system basis, the trend comparison for PBE+U_{eff} versus r^{2}SCAN is favorable in that the $T_{1/2}$ results are moved closer to experiment without the significantly greater cost in computing resources and user management required for r^{2}SCAN.

It also is important to highlight that results with the PBE +U_{eff} approximation compete in accuracy with those reported for isolated molecules using the global hybrid TPSSh,[52,104] that includes 10% of computationally costly single determinant exchange. However, transition temperatures with either PBE +U_{eff}, r^{2}SCAN, or TPSSh still are twice as large as those computed for isolated molecules with the empirically calibrated B3LYP* density functional,[105] that mixes 15% of single determinant exchange instead, resulting in ΔE_{HL} closer to the experimental reference. In this sense, the combination of mean-value-ensemble U_{eff} and the first coordination sphere approximation is of significant potential value for system screening. Moreover, since the mean value ensemble method does not depend upon fitting to experimental data for the calculation of the U_{eff} parameters and it provides a more reasonable correction to ΔE_{HL},[70] the methodology may be attractive for use with automated high-demanding workflows for materials research, targeted to identifying potential spin transition materials. Further studies could then use computationally expensive methodologies, e.g., r^{2}SCAN, range-separated or local hybrids, *GW*,[106] to achieve a better understanding of these individual systems.

CONCLUSION

We discussed three sources of uncertainties for the calculation of transition temperatures, namely, at least 100 to 150 K whether the computation relies on isolated molecules or the crystalline phase, an additional 50 K from the magnitude of the Hubbard-*U* parameter, and a system-dependent uncertainty from the choice of coordination shell approximation for the computation of the vibrational contributions to the Gibbs free energy.

Assessment of the Hubbard-*U* mean value ensemble method on the thermodynamic evolution for a set of experimental spin transition materials revealed that the PBE+U_{eff} approximation provides results with an accuracy comparable to that obtained with the more elaborate r^{2}SCAN density functional approximation. Their mean absolute error and root-mean-square error differ by 6 and 114 K, respectively, in favor of r^{2}SCAN.

Overall, we suggest that the improvement in $T_{1/2}$ observed for PBE+U_{eff}, compared to the uncorrected PBE density functional approximation, may provide a computationally feasible, non-empirical, alternative for efficient high-throughput screening, as well as identification, of spin-crossover materials for later refinement with more sophisticated electronic structure approaches.

AUTHOR INFORMATION

Corresponding Authors

Richard G. Hennig − *Center for Molecular Magnetic Quantum Materials, Quantum Theory Project, University of Florida, Gainesville, Florida 32611, United States; Department of Materials Science and Engineering, University of Florida, Gainesville, Florida 32611, United States;* orcid.org/0000-0003-4933-7686; Email: rhennig@ufl.edu

S. B. Trickey − *Center for Molecular Magnetic Quantum Materials, Quantum Theory Project, University of Florida, Gainesville, Florida 32611, United States; Department of Physics and Department of Chemistry, University of Florida, Gainesville, Florida 32611, United States;* orcid.org/0000-0001-9224-6304; Email: trickey@ufl.edu

Author

Angel Albavera-Mata − *Center for Molecular Magnetic Quantum Materials, Quantum Theory Project, University of Florida, Gainesville, Florida 32611, United States; Department of Materials Science and Engineering, University of Florida, Gainesville, Florida 32611, United States;* orcid.org/0000-0003-1521-678X

Complete contact information is available at: https://pubs.acs.org/10.1021/acs.jpca.3c03520

Notes

The authors declare no competing financial interest.

ACKNOWLEDGMENTS

This work was supported as part of the Center for Molecular Magnetic Quantum Materials, an Energy Frontier Research Center funded by the U.S. Department of Energy, Office of Science, Basic Energy Sciences, under Award No. DE-SC0019330.

REFERENCES

(1) Gütlich, P.; Goodwin, H. A. *Spin Crossover in Transition Metal Compounds I*; Springer: Berlin, Heidelberg, Germany, 2004; pp 1−47.

(2) Kepp, K. P. In *Transition Metals in Coordination Environments: Computational Chemistry and Catalysis Viewpoints*; Broclawik, E., Borowski, T., Radoń, M., Eds.; Springer International Publishing: Cham, Switzerland, 2019; pp 1−33.

(3) McQuarrie, D. A. *Statistical Mechanics*; Harper and Row: New York, 1976; pp 35−64.

(4) Ewing, J. A. On the Production of Transient Electric Currents in Iron and Steel Conductors by Twisting Them When Magnetised or by Magnetising Them When Twisted. *Proc. R. Soc. London* **1882**, *33*, 21−23.

(5) Brooker, S. Spin Crossover with Thermal Hysteresis: Practicalities and Lessons Learnt. *Chem. Soc. Rev.* **2015**, *44*, 2880−2892.

(6) Oshio, H.; Toriumi, K.; Maeda, Y.; Takashima, Y. Temperature-Dependent Crystallographic Studies on Ferric Spin-Crossover Complexes with Different Spin-Interconversion Rates. *Inorg. Chem.* **1991**, *30*, 4252−4260.

(7) Gütlich, P. Thermal and Optical Switching of Bistable Iron Compounds and Possible Applications. *Nucl. Instrum. Methods Phys. Res. B: Beam Interact. Mater. At.* **1993**, *76*, 387−396.

(8) Toftlund, H. Spin Equilibrium in Solutions. *Monatsh. Chem.* **2001**, *132*, 1269−1277.

(9) Kepp, K. P. Consistent Descriptions of Metal-Ligand Bonds and Spin-Crossover in Inorganic Chemistry. *Coord. Chem. Rev.* **2013**, *257*, 196−209.

https://doi.org/10.1021/acs.jpca.3c03520
J. Phys. Chem. A 2023, 127, 7646−7654

(10) Hayami, S.; Gu, Z.-z.; Yoshiki, H.; Fujishima, A.; Sato, O. Iron(III) Spin-Crossover Compounds with a Wide Apparent Thermal Hysteresis Around Room Temperature. *J. Am. Chem. Soc.* **2001**, *123*, 11644−11650.
(11) Bonhommeau, S.; Molnár, G.; Galet, A.; Zwick, A.; Real, J.-A.; McGarvey, A. J.; Bousseksou, A. One Shot Laser Pulse Induced Reversible Spin Transition in the Spin-Crossover Complex $[Fe(C_4H_4N_2)\{Pt(CN)_4\}]$ at Room Temperature. *Angew. Chem., Int. Ed.* **2005**, *44*, 4069−4073.
(12) Cobo, S.; Molnár, G.; Real, J. A.; Bousseksou, A. Multilayer Sequential Assembly of Thin Films that Display Room-Temperature Spin Crossover with Hysteresis. *Angew. Chem., Int. Ed.* **2006**, *45*, 5786−5789.
(13) Coronado, E.; Galán-Mascarós, J. R.; Monrabal-Capilla, M.; García-Martínez, J.; Pardo-Ibáñez, P. Bistable Spin-Crossover Nanoparticles Showing Magnetic Thermal Hysteresis Near Room Temperature. *Adv. Mater.* **2007**, *19*, 1359−1361.
(14) Boldog, I.; Gaspar, A. B.; Martínez, V.; Pardo-Ibañez, P.; Ksenofontov, V.; Bhattacharjee, A.; Gütlich, P.; Real, J. A. Spin-Crossover Nanocrystals with Magnetic, Optical, and Structural Bistability Near Room Temperature. *Angew. Chem., Int. Ed.* **2008**, *47*, 6433−6437.
(15) Cobo, S.; Ostrovskii, D.; Bonhommeau, S.; Vendier, L.; Molnár, G.; Salmon, L.; Tanaka, K.; Bousseksou, A. Single-Laser-Shot-Induced Complete Bidirectional Spin Transition at Room Temperature in Single Crystals of $(Fe^{II}(pyrazine)(Pt(CN)_4$. *J. Am. Chem. Soc.* **2008**, *130*, 9019−9024.
(16) Prins, F.; Monrabal-Capilla, M.; Osorio, E. A.; Coronado, E.; van der Zant, H. S. J. Room-Temperature Electrical Addressing of a Bistable Spin-Crossover Molecular System. *Adv. Mater.* **2011**, *23*, 1545−1549.
(17) Durand, P.; Pillet, S.; Bendeif, E.-E.; Carteret, C.; Bouazaoui, M.; Hamzaoui, H. E.; Capoen, B.; Salmon, L.; Hébert, S.; Ghanbaja, J.; et al. Room Temperature Bistability with Wide Thermal Hysteresis in a Spin Crossover Silica Nanocomposite. *J. Mater. Chem. C* **2013**, *1*, 1933−1942.
(18) Fitzpatrick, A. J.; Martinho, P. N.; Gildea, B. J.; Holbrey, J. D.; Morgan, G. G. Robust Room Temperature Hysteresis in an Fe(III) Spin Crossover Metallomesogen. *Eur. J. Inorg. Chem.* **2016**, *2016*, 2025−2029.
(19) Khusniyarov, M. M. How to Switch Spin-Crossover Metal Complexes at Constant Room Temperature. *Chem. Eur. J.* **2016**, *22*, 15178−15191.
(20) Hardy, M.; Tessarolo, J.; Holstein, J. J.; Struch, N.; Wagner, N.; Weisbarth, R.; Engeser, M.; Beck, J.; Horiuchi, S.; Clever, G. H.; et al. A Family of Heterobimetallic Cubes Shows Spin-Crossover Behaviour Near Room Temperature. *Angew. Chem., Int. Ed.* **2021**, *60*, 22562−22569.
(21) Kahn, O.; Kröber, J.; Jay, C. Spin Transition Molecular Materials for Displays and Data Recording. *Adv. Mater.* **1992**, *4*, 718−728.
(22) Kahn, O.; Martinez, C. J. Spin-Transition Polymers: From Molecular Materials Toward Memory Devices. *Science* **1998**, *279*, 44−48.
(23) Garcia, Y.; Ksenofontov, V.; Gütlich, P. Spin Transition Molecular Materials: New Sensors. *Hyperfine Interact.* **2002**, *139*, 543−551.
(24) Muller, R. N.; Vander, E. L.; Laurent, S. Spin Transition Molecular Materials: Intelligent Contrast Agents for Magnetic Resonance Imaging. *J. Am. Chem. Soc.* **2003**, *125*, 8405−8407.
(25) Létard, J.-F.; Guionneau, P.; Goux-Capes, L. In *Spin Crossover in Transition Metal Compounds*; Gütlich, P., Goodwin, H. A., Eds.; Springer: Berlin, Heidelberg, Germany, 2004; pp 221−249.
(26) Larionova, J.; Salmon, L.; Guari, Y.; Tokarev, A.; Molvinger, K.; Molnár, G.; Bousseksou, A. Towards the Ultimate Size Limit of the Memory Effect in Spin-Crossover Solids. *Angew. Chem., Int. Ed.* **2008**, *47*, 8236−8240.
(27) Sanvito, S. Molecular Spintronics. *Chem. Soc. Rev.* **2011**, *40*, 3336−3355.
(28) Quintero, C. M.; Félix, G.; Suleimanov, I.; Sánchez, C. J.; Molnár, G.; Salmon, L.; Nicolazzi, W.; Bousseksou, A. Hybrid Spin-Crossover Nanostructures. *Beilstein J. Nanotechnol.* **2014**, *5*, 2230−2239.
(29) Ruiz, E. Charge Transport Properties of Spin Crossover Systems. *Phys. Chem. Chem. Phys.* **2014**, *16*, 14−22.
(30) Jureschi, C. M.; Linares, J.; Rotaru, A.; Ritti, M. H.; Parlier, M.; Dîrtu, M. M.; Wolff, M.; Garcia, Y. Pressure Sensor via Optical Detection Based on a 1D Spin Transition Coordination Polymer. *Sensors* **2015**, *15*, 2388−2398.
(31) Manrique-Juárez, M. D.; Rat, S.; Salmon, L.; Molnár, G.; Quintero, C. M.; Nicu, L.; Shepherd, H. J.; Bousseksou, A. Switchable Molecule-Based Materials for Micro- and Nanoscale Actuating Applications: Achievements and Prospects. *Coord. Chem. Rev.* **2016**, *308*, 395−408.
(32) Mikolasek, M.; Manrique-Juarez, M. D.; Shepherd, H. J.; Ridier, K.; Rat, S.; Shalabaeva, V.; Bas, A.-C.; Collings, I. E.; Mathieu, F.; Cacheux, J.; et al. Complete Set of Elastic Moduli of a Spin-Crossover Solid: Spin-State Dependence and Mechanical Actuation. *J. Am. Chem. Soc.* **2018**, *140*, 8970−8979.
(33) Cruddas, J.; Powell, B. J. Multiple Coulomb Phases with Temperature-Tunable Ice Rules in Pyrochlore Spin-Crossover Materials. *Phys. Rev. B* **2021**, *104*, 024433.
(34) Nadeem, M.; Cruddas, J.; Ruzzi, G.; Powell, B. J. Toward High-Temperature Light-Induced Spin-State Trapping in Spin-Crossover Materials: The Interplay of Collective and Molecular Effects. *J. Am. Chem. Soc.* **2022**, *144*, 9138−9148.
(35) Demuth, M. C.; Le, K. N.; Sciprint, M.; Hendon, C. H. Ligand-Engineered Spin Crossover in Fe(II)-Based Molecular and Metal-Organic Framework Systems. *J. Phys. Chem. C* **2023**, *127*, 2735−2740.
(36) Kohn, W.; Sham, L. J. Self-Consistent Equations Including Exchange and Correlation Effects. *Phys. Rev.* **1965**, *140*, A1133.
(37) Engel, E.; Dreizler, R. M. *Density Functional Theory*; Springer: Heidelberg, Germany, 2013.
(38) Becke, A. D. A New Mixing of Hartree-Fock and Local Density-Functional Theories. *J. Chem. Phys.* **1993**, *98*, 1372−1377.
(39) Savin, A.; Flad, H.-J. Density Functionals for the Yukawa Electron-Electron Interaction. *Int. J. Quantum Chem.* **1995**, *56*, 327−332.
(40) Gill, P. M. W.; Adamson, R. D.; Pople, J. A. Coulomb-Attenuated Exchange Energy Density Functionals. *Mol. Phys.* **1996**, *88*, 1005−1009.
(41) Jaramillo, J.; Scuseria, G. E.; Ernzerhof, M. Local Hybrid Functionals. *J. Chem. Phys.* **2003**, *118*, 1068−1073.
(42) Hubbard, J. Electron Correlations in Narrow Energy Bands. *Proc. R. Soc. London A* **1963**, *276*, 238−257.
(43) Anisimov, V. I.; Zaanen, J.; Andersen, O. K. Band Theory and Mott Insulators: Hubbard U Instead of Stoner I. *Phys. Rev. B* **1991**, *44*, 943−954.
(44) Nicolazzi, W.; Bousseksou, A. Thermodynamical Aspects of the Spin Crossover Phenomenon. *C. R. Chimie* **2018**, *21*, 1060−1074.
(45) McQuarrie, D. A.; Simon, J. D. *Molecular Thermodynamics*; University Science Books: Sausalito, CA, 1999; pp 143−168.
(46) Wolny, J. A.; Paulsen, H.; Trautwein, A. X.; Schünemann, V. Density Functional Theory Calculations and Vibrational Spectroscopy on Iron Spin-Crossover Compounds. *Coord. Chem. Rev.* **2009**, *253*, 2423−2431.
(47) Cirera, J.; Paesani, F. Theoretical Prediction of Spin-Crossover Temperatures in Ligand-Driven Light-Induced Spin Change Systems. *Inorg. Chem.* **2012**, *51*, 8194−8201.
(48) Matouzenko, G. S.; Borshch, S. A.; Schünemann, V.; Wolny, J. A. Ligand Strain and Conformations in a Family of Fe(II) Spin Crossover Hexadentate Complexes Involving the 2-pyridylmethylamino Moiety: DFT Modelling. *Phys. Chem. Chem. Phys.* **2013**, *15*, 7411−7419.
(49) Rudavskyi, A.; Sousa, C.; de Graaf, C.; Havenith, R. W. A.; Broer, R. Computational Approach to the Study of Thermal Spin Crossover Phenomena. *J. Chem. Phys.* **2014**, *140*, 184318.

https://doi.org/10.1021/acs.jpca.3c03520
J. Phys. Chem. A 2023, 127, 7646−7654

(50) Slimani, A.; Yu, X.; Boukheddaden, A. M.; Yamashita, K.; Reparametrization, K. Approach of DFT Functionals Based on the Equilibrium Temperature of Spin-Crossover Compounds. *J. Phys. Chem. A* **2014**, *118*, 9005−9012.
(51) Kimura, A.; Ishida, T. Spin-Crossover Temperature Predictable from DFT Calculation for Iron(II) Complexes with 4-Substituted Pybox and Related Heteroaromatic Ligands. *ACS Omega* **2018**, *3*, 6737−6757.
(52) Cirera, J.; Via-Nadal, M.; Ruiz, R. Benchmarking Density Functional Methods for Calculation of State Energies of First Row Spin-Crossover Molecules. *Inorg. Chem.* **2018**, *57*, 14097−14105.
(53) Cirera, J.; Ruiz, E. Computational Modeling of Transition Temperatures in Spin-Crossover Systems. Comments. *Inorg. Chem.* **2019**, *39*, 216−241.
(54) Ishida, T.; Ito, S.; Homma, Y.; Kyoden, Y. Molecular S = 2 High-Spin, S = 0 Low-Spin and S = 0⇆2 Spin-Transition/-Crossover Nickel(II)-Bis(nitroxide) Coordination Compounds. *Inorganics* **2021**, *9*, 10.
(55) Janetzki, J. T.; Zahir, F. Z. M.; Gable, R. W.; Phonsri, W.; Murray, K. S.; Goerigk, L.; Boskovic, C. A Convenient DFT-Based Strategy for Predicting Transition Temperatures of Valence Tautomeric Molecular Switches. *Inorg. Chem.* **2021**, *60*, 14475−14487.
(56) Sharp, R. T.; Horton, G. K. A Variational Approach to the Unipotential Many-Electron Problem. *Phys. Rev.* **1953**, *90*, 317.
(57) Talman, J. D.; Shadwick, W. F. Optimized Effective Atomic Central Potential. *Phys. Rev. A* **1976**, *14*, 36.
(58) Sahni, V.; Gruenebaum, J.; Perdew, J. P. Study of the Density-Gradient Expansion for the Exchange Energy. *Phys. Rev. B* **1982**, *26*, 4371.
(59) Wu, Z.; Justo, J. F.; da Silva, C. R. S.; de Gironcoli, S.; Wentzcovitch, R. M. Anomalous Thermodynamic Properties in Ferropericlase Throughout its Spin Crossover. *Phys. Rev. B* **2009**, *80*, 014409.
(60) Zhang, Y. Predicting Critical Temperatures of Iron(II) Spin Crossover Materials: Density Functional Theory Plus U Approach. *J. Chem. Phys.* **2014**, *141*, 214703.
(61) Vela, S.; Fumanal, M.; Ribas-Arinob, J.; Robert, V. Towards an Accurate and Computationally-Efficient Modelling of Fe(II)-Based Spin Crossover Materials. *Phys. Chem. Chem. Phys.* **2015**, *17*, 16306−16314.
(62) Zhang, Y. Calculating Spin Crossover Temperatures by a First-Principles LDA+U Scheme with Parameter U Evaluated from GW. *J. Chem. Phys.* **2019**, *151*, 134701.
(63) Ohlrich, M.; Powell, B. J. Fast, Accurate Enthalpy Differences in Spin Crossover Crystals from DFT+U. *J. Chem. Phys.* **2020**, *153*, 104107.
(64) Pickett, W. E.; Erwin, S. C.; Ethridge, E. C. Reformulation of the LDA+U Method for a Local-Orbital Basis. *Phys. Rev. B* **1998**, *58*, 1201.
(65) Cococcioni, M.; de Gironcoli, S. Linear Response Approach to the Calculation of the Effective Interaction Parameters in the LDA+U Method. *Phys. Rev. B* **2005**, *71*, 035105.
(66) Kulik, H. J.; Cococcioni, M.; Scherlis, D. A.; Marzari, N. Density Functional Theory in Transition-Metal Chemistry: A Self-Consistent Hubbard U Approach. *Phys. Rev. Lett.* **2006**, *97*, 103001.
(67) Himmetoglu, B.; Floris, A.; de Gironcoli, S.; Cococcioni, M. Hubbard-Corrected DFT Energy Functionals: The LDA+U Description of Correlated Systems. *Int. J. Quantum Chem.* **2014**, *114*, 14−49.
(68) Linscott, E. B.; Cole, D. J.; Payne, M. C.; O'Regan, D. D. Role of Spin in the Calculation of Hubbard U and Hund's J Parameters from First Principles. *Phys. Rev. B* **2018**, *98*, 235157.
(69) Mejía-Rodríguez, D.; Albavera-Mata, A.; Fonseca, E.; Chen, D.; Cheng, H.-P.; Hennig, R. G.; Trickey, S. B. Barriers to Predictive High-Throughput Screening for Spin-Crossover. *Comput. Mater. Sci.* **2022**, *206*, 111161.
(70) Albavera-Mata, A.; Trickey, S.B.; Hennig, R.G. Mean Value Ensemble Hubbard-U Correction for Spin-Crossover Molecules. *J. Phys. Chem. Lett.* **2022**, *13*, 12049−12054.
(71) Perdew, J. P.; Burke, K.; Ernzerhof, M. Generalized Gradient Approximation Made Simple. *Phys. Rev. Lett.* **1996**, *77*, 3865.
(72) Perdew, J. P.; Burke, K.; Ernzerhof, M. Generalized Gradient Approximation Made Simple [Phys. Rev. Lett. 77, 3865 (1996)]. *Phys. Rev. Lett.* **1997**, *78*, 1396.
(73) Harding, D. J.; Phonsri, W.; Harding, P.; Murray, K. S.; Moubaraki, B.; Jameson, G. N. L. Abrupt Two-Step and Symmetry Breaking Spin Crossover in an Iron(III) Complex: an Exceptionally Wide [LS-HS] Plateau. *Dalton Trans.* **2015**, *44*, 15079−15082.
(74) Halepoto, D. M.; Holt, D. G. L.; Larkworthy, L. F.; Leigh, G. J.; Povey, D. C.; Smith, G. W. Spin Crossover in Chromium(II) Complexes and the Crystal and Molecular Structure of the High Spin Form of Bis[1,2-bis(diethylphosphino)ethane]di-iodochromium(II). *J. Chem. Soc., Chem. Commun.* **1989**, *18*, 1322−1323.
(75) Sim, P. G.; Sinn, E. First Manganese(III) Spin Crossover, First d4 Crossover. Comment on Cytochrome Oxidase. *J. Am. Chem. Soc.* **1981**, *103*, 241−243.
(76) Pandurangan, K.; Gildea, B.; Murray, C.; Harding, C. J.; Müller-Bunz, H.; Morgan, G. G. Lattice Effects on the Spin-Crossover Profile of a Mononuclear Manganese(III) Cation. *Chem. Eur. J.* **2012**, *18*, 2021−2029.
(77) Martinho, P. N.; Gildea, B.; Harris, M. M.; Lemma, T.; Naik, A. D.; Müller-Bunz, H.; Keyes, T. E.; Garcia, Y.; Morgan, G. G. Cooperative Spin Transition in a Mononuclear Manganese(III) Complex. *Angew. Chem., Int. Ed.* **2012**, *51*, 12597−12601.
(78) Switzer, M. E.; Wang, R.; Rettig, M. F.; Maki, A. H. Electronic Ground States of Manganocene and 1,1'-dimethylmanganocene. *J. Am. Chem. Soc.* **1974**, *96*, 7669−7674.
(79) Walter, M. D.; Sofield, C. D.; Booth, C. H.; Andersen, R. A. Spin Equilibria in Monomeric Manganocenes: Solid-State Magnetic and EXAFS Studies. *Organometallics* **2009**, *28*, 2005−2019.
(80) Sinn, E.; Sim, G.; Dose, E. V.; Tweedle, M. F.; Wilson, L. J. Iron(III) Chelates with Hexadentate Ligands from triethylenetetramine and .beta.-diketones or Salicylaldehyde. Spin State Dependent Crystal and Molecular Structures of [Fe(acac)2trien]PF6(S = 5/2), [Fe(acacCl)2trien]PF6(S = 5/2), [Fe(sal)2trien]Cl.2H2O(S = 1/2), and [Fe(sal)2trien]NO3.H2O(S = 1/2). *J. Am. Chem. Soc.* **1978**, *100*, 3375−3390.
(81) Maeda, Y.; Oshio, H.; Toriumi, K.; Takashima, Y. Crystal Structures, Mössbauer Spectra and Magnetic Properties of Two Iron(III) Spin-Crossover Complexes. *J. Chem. Soc., Dalton Trans.* **1991**, *5*, 1227−1235.
(82) Tissot, A.; Bertoni, R.; Collet, E.; Toupet, L.; Boillot, M.-L. The Cooperative Spin-State Transition of an Iron(III) Compound [FeIII(3-MeO-SalEen)2]PF6: Thermal- vs. Ultra-Fast Photo-Switching. *J. Mater. Chem.* **2011**, *21*, 18347−18353.
(83) Gallois, B.; Real, J. A.; Hauw, C.; Zarembowitch, J. Structural Changes Associated with the Spin Transition in Bis(isothiocyanato)-bis(1,10-phenanthroline)iron: A Single-Crystal X-ray Investigation. *Inorg. Chem.* **1990**, *29*, 1152−1158.
(84) Roux, C.; Zarembowitch, J.; Gallois, B.; Granier, T.; Claude, R. Toward Ligand-Driven Light-Induced Spin Changing. Influence of the Configuration of 4 Styrylpyridine (stpy) on the Magnetic Properties of FeII(stpy)4(NCS)2 Complexes. Crystal Structures of the Spin-Crossover Species Fe(trans-stpy)4(NCS)2 and of the High-Spin Species Fe(cis-stpy)4(NCS)2. *Inorg. Chem.* **1994**, *33*, 2273−2279.
(85) Carbonera, C.; Kilner, C. A.; Létard, J.-F.; Halcrow, M. A. Anion Doping as a Probe of Cooperativity in the Molecular Spin-Crossover Compound [FeL2][BF4]2 (L = 2,6-dipyrazol-1-ylpyridine). *Dalton Trans.* **2007**, *3*, 1284−1292.
(86) Real, J. A.; Muñoz, M. C.; Faus, J.; Solans, X. Spin Crossover in Novel Dihydrobis(1-pyrazolyl)borate [H2B(pz)2]-Containing Iron(II) Complexes. Synthesis, X-ray Structure, and Magnetic Properties of [FeLH2B(pz)22] (L = 1,10-Phenanthroline and 2,2'-Bipyridine). *Inorg. Chem.* **1997**, *36*, 3008−3013.
(87) Niel, V.; Gaspar, A. B.; Muñoz, M. C.; Abarca, B.; Ballesteros, R.; Real, J. A. Spin Crossover Behavior in the Iron(II)-2-pyridyl-[1,2,3]triazolo[1,5-a]pyridine System: X-ray Structure, Calorimetric,

https://doi.org/10.1021/acs.jpca.3c03520
J. Phys. Chem. A 2023, 127, 7646−7654

Magnetic, and Photomagnetic Studies. *Inorg. Chem.* **2003**, *42*, 4782−4788.
(88) Figgis, B. N.; Kucharski, E. S.; White, A. H. Crystal Structure of Bis(2,2':6',2"-terpyridyl)cobalt(II) Iodide Dihydrate at 295 K and at 120 K. *Aust. J. Chem.* **1983**, *36*, 1527−1535.
(89) Charpin, P.; Nierlich, M.; Vigner, D.; Lance, M.; Thuery, P.; Zarembowitch, J.; D'yvoire, F. Crystal and Molecular Structure of the Spin-Crossover Complex Bis(pyridine) [N,N'-ethylenebis (3-carboxysalicylaldimine)] Cobalt (II). *J. Crystallogr. Spectrosc. Res.* **1988**, *18*, 429−437.
(90) Gaspar, A. B.; Muñoz, M. C.; Niel, V.; Real, J. A. [CoII(4-terpyridone)2]X2: A Novel Cobalt(II) Spin Crossover System [4-Terpyridone = 2,6-Bis(2-pyridyl)-4(1H)-pyridone]. *Inorg. Chem.* **2001**, *40*, 9−10.
(91) Taylor, R. A.; Lough, A. J.; Lemaire, M. T. Spin-Crossover in a Homoleptic Cobalt(II) Complex Containing a Redox-Active NNO Ligand. *J. Mater. Chem. C* **2016**, *4*, 455−459.
(92) Hayami, S.; Nakaya, M.; Ohmagari, H.; Alao, A. S.; Nakamura, M.; Ohtani, R.; Yamaguchi, R.; Kuroda-Sowa, T.; Clegg, J. K. Spin-Crossover Behaviors in Solvated Cobalt(II) Compounds. *Dalton Trans.* **2015**, *44*, 9345−9348.
(93) Kresse, G.; Furthmüller, J. Efficient Iterative Schemes for Ab Initio Total-Energy Calculations Using a Plane-Wave Basis Set. *Phys. Rev. B* **1996**, *54*, 11169.
(94) Furness, J. W.; Kaplan, A. D.; Nig, J.; Perdew, J. P.; Sun, J. Accurate and Numerically Efficient r^{2}SCAN meta-Generalized Gradient Approximation. *J. Phys. Chem. Lett.* **2020**, *11*, 8208−8215.
(95) Perdew, J. P.; Ruzsinszky, A.; Csonka, G. I.; Vydrov, O. A.; Scuseria, G. E.; Constantin, L. A.; Zhou, X.; Burke, K. Restoring the Density-Gradient Expansion for Exchange in Solids and Surfaces. *Phys. Rev. Lett.* **2008**, *100*, 136406.
(96) Perdew, J. P.; Ruzsinszky, A.; Csonka, G. I.; Vydrov, O. A.; Scuseria, G. E.; Constantin, L. A.; Zhou, X.; Burke, K. Erratum: Restoring the Density-Gradient Expansion for Exchange in Solids and Surfaces [Phys. Rev. Lett. 100, 136406 (2008)]. *Phys. Rev. Lett.* **2009**, *102*, 039902.
(97) Holmström, E.; Stixrude, L. Spin Crossover in Ferropericlase from First-Principles Molecular Dynamics. *Phys. Rev. Lett.* **2015**, *114*, 117202.
(98) Barreda-Argüeso, J. E.; Nataf, L.; Aguado, F.; et al. Pressure-Induced Spin Transition and Site-Selective Metallization in $CoCl_2$. *Sci. Rep.* **2019**, *9*, 5448.
(99) Gakiya-Teruya, M.; Jiang, X.; Le, D.; Üngör, Ö; Durrani, A. J.; Koptur-Palenchar, J. J.; Jiang, J.; Jiang, T.; Meisel, M. W.; Cheng, H.-P.; et al. Asymmetric Design of Spin-Crossover Complexes to Increase the Volatility for Surface Deposition. *J. Am. Chem. Soc.* **2021**, *143*, 14563−14572.
(100) Sanchez, J. M.; Ducastelle, F.; Gratias, D. Generalized Cluster Description of Multicomponent Systems. *Physica A* **1984**, *128*, 334−350.
(101) Laks, D. B.; Ferreira, L. G.; Froyen, S.; Zunger, A. Efficient Cluster Expansion for Substitutional Systems. *Phys. Rev. B* **1992**, *46*, 12587.
(102) De Fontaine, D. Cluster Approach to Order-Disorder Transformations in Alloys. *Solid State Phys.* **1994**, *47*, 33−176.
(103) van de Walle, A. A Complete Representation of Structure-Property Relationships in Crystals. *Nat. Mater.* **2008**, *7*, 455−458.
(104) Cirera, J.; Ruiz, E. Assessment of the SCAN Functional for Spin-State Energies in Spin-Crossover Systems. *J. Phys. Chem. A* **2020**, *124*, 5053−5058.
(105) Vidal, D.; Cirera, J.; Ribas-Arino, J. Accurate Calculation of Spin-State Energy Gaps in Fe(III) Spin-Crossover Systems Using Density Functional Methods. *Dalton Trans.* **2021**, *50*, 17635−17642.
(106) Hybertsen, M. S.; Louie, S. G. Electron Correlation in Semiconductors and Insulators: Band Gaps and Quasiparticle Energies. *Phys. Rev. B* **1986**, *34*, 5390−5413.

https://doi.org/10.1021/acs.jpca.3c03520
J. Phys. Chem. A 2023, 127, 7646−7654